PEER REVIEWED

Tribological Performance of Thin HVAF-Sprayed WC-CoCr Coatings Fabricated Employing Fine Powder Feedstock

Kaveh Torkashvand[1] · Mohit Gupta[1] · Stefan Björklund[1] · Shrikant Joshi[1]

Abstract In this study, sliding and abrasion wear performance of WC-CoCr coatings deposited by high velocity air–fuel (HVAF) spraying with various thicknesses (i.e., 240, 150, 100, 50 and 30 μm), fabricated from fine feedstock powder (5–15 μm), were evaluated. The main aim was to investigate how thinner coatings (30 and 50 μm) perform compared to conventional thick coatings (> 100 μm), in an effort to address the supply and cost concerns associated with Co and W. The feedstock powder and deposited coatings were characterized in terms of microstructure. The hardness of the thin and thick coatings was measured using Vickers hardness method from both cross section and top-surface. It was found that, regardless of the thickness, extremely dense coatings with very high hardness ($\sim$ 1500 HV) can be deposited employing HVAF and fine feedstock powder. Thin and thick coatings were found to perform similarly under sliding wear with a normal load of 10 N or lower as well as under abrasion wear conditions which highlights the possibility of employing thinner coatings for a majority of the real applications. The results suggest that peening effect does not have a considerable influence on the microstructure or performance of the deposited coatings. However, for sliding wear tests with a 20 N normal load, it was noticed that wear resistance of the coatings slightly declines with decreasing thickness of the coating beyond 150 μm. The main reason was identified to be the involvement of substrate effect when performing tests under severe Hertzian contact pressure.

✉ Kaveh Torkashvand
kaveh.torkashvand@hv.se

1   Department of Engineering Science, University West,
Trollhättan, Sweden

Keywords abrasion · coatings · HVAF · sliding wear · thickness · WC-CoCr

Introduction

When it comes to surface engineering for tribological applications, WC-based coatings, deposited by thermal spray techniques, are recognized as one of the most promising solutions to combat wear (Ref 1, 2). A combination of very high hardness and toughness in these cermet coatings yields excellent performance under severe wear conditions (Ref 3, 4). The high toughness of the coating system is thanks to the addition of around 12–15 wt% (20–30 vol%) of metallic binder, which is conventionally Co (Ref 5) or Co with some addition of Cr for oxidation resistance property at relatively high temperatures (Ref 6). These coatings can be deposited employing various thermal spray techniques, among which high velocity oxy-fuel (HVOF) and high velocity air–fuel (HVAF) spraying methods have been considered more attractive. This is due to a generally suitable in-flight particle velocity and temperature achieved in these techniques, which not only yields a very dense coating microstructure but also minimizes the extent of decarburization (Ref 7, 8).

Comparing HVOF and HVAF spraying methods, HVAF typically provides higher kinetic energy and lower flame temperature because of employing compressed air in this method (rather than oxygen) which has a lower combustion potential compared to oxygen (Ref 9, 10). In other words, this technique enables particles to reach very high in-flight velocity while their temperature does not exceed 1500 °C. Keeping the in-flight temperature low is specifically desirable since it prevents decarburization in WC-based coatings (Ref 11, 12). Decarburization can be more

pronounced when using finer particles (below 20 μm) because of higher specific surface area in a way that the core of the particles can also reach temperatures above the melting point. For instance, employing a modeling technique, it was shown that WC-CoCr powder particles, with sizes smaller than 15 μm, became fully molten when their surface temperature exceeded 1800 °C (Ref 13, 14). Nonetheless, powder feedstock with finer size distribution is desired in some cases since it can improve microstructural characteristics like density, mechanical properties such as hardness as well as tribological performance (Ref 15). The HVAF technique is best suited for spraying fine WC-based powders without excessive decarburization (Ref 15, 16). This also paves the way to produce coatings with fine microstructures, improved mechanical properties and tribological performance. Moreover, fine feedstock powders sprayed by HVAF technique can potentially result in a better coating uniformity in terms of carbide distribution as well as a lower surface roughness which can lead to reduced effort and cost in finish grinding of coated parts.

A typical thickness of 200–300 μm is generally targeted for WC-based coatings deposited employing thermal spray methods (Ref 2, 17). However, deposition of thinner coatings with improved properties could be feasible thanks to HVAF technique, viable to process fine (5–15 μm) powders. The fabrication of a thinner coating is more favorable from processing time and economical aspects. Fabrication of thinner coating is even more crucial when using WC-CoCr as feedstock powder, considering supply risk concerns around both W and Co elements (Ref 18, 19) as well as environmental concerns around Co (Ref 20, 21). Reducing coating thickness from a typical 200–50 μm, therefore, can reduce the usage of these elements by a factor of four. Several research studies have been carried out to investigate properties and wear performance of these thick coatings (Ref 15, 22, 23). However, the influence of coating thickness, as an important aspect, has not been explicitly explored in previous studies. Investigating influence of thickness is crucial from various aspects. Coating thickness can potentially influence wear performance, especially when dealing with soft substrates. High Hertzian contact stresses can be induced to coating/substrate system as a result of contact with a rigid ball as the counterpart. Depending on the coating's thickness as well as contact conditions, the maximum Hertzian stress could locate within the coating or substrate (Ref 24). When coating's thickness is less than a critical value, a great portion of the applied stress has to be carried by the substrate thereby, thin hard coatings applied on soft substrates are susceptible to fracture due to substrate deformation (Ref 25). It has been investigated that by an increase in thickness and as a result shifting the stresses away from the interface and toward the coating system, thermal spray

coatings exhibit better rolling contact fatigue (Ref 26, 27). Also, in a study by Bolelli et al. (Ref 28), it was shown that sliding wear performance could be improved by increasing the number of torch passes in a HVOF WC-CoCr coating (increase in thickness). This can be exceptionally critical when dealing with thinner coatings (< 50 μm) since a large portion of the concentrated stress from the counterpart can be directed to the substrate. Another important factor to consider is peening effect and its influence on wear performance of the coating. When spraying a thinner coating, the sub-layers are exposed to fewer spray strokes (i.e., fewer hard particles impacting the surface) and consequently a less pronounced effect of peening.

Influence of substrate is another key factor. The role of substrate can start to come into the picture when dealing with thinner coatings, especially when the substrate is considerably softer than the protective coating. There is no extensive study investigating this in the literature about the potential influence of substrate and its extent on the coating performance. In this paper, a comprehensive investigation is conducted on coatings fabricated from fine powder (5–15 μm) with different thicknesses, ranging from 30 μm (thin) to 240 μm (thick), to evaluate their characteristics and wear performance under sliding and abrasive wear conditions. Also, the results were compared with coatings fabricated from coarse powder (15–45 μm) where relevant.

Experiment Procedure

Spraying Process

Commercially available WC-10Co4Cr powder produced by Höganäs GmbH, with a particle size range of 5–15 μm, manufactured employing agglomeration and sintering processing technique (trade name: Amperit® 558.090) was used as feedstock material. Domex® 355MC HSLA Steel (hot-rolled sheet steel produced by SSAB) coupons (ϕ = 25.4 mm and thickness of 6 mm) and plates (70 × 25 × 6 mm) were employed as the substrate for sliding wear and abrasion wear, respectively.

An M2 HVAF torch (Uniquecoat Technologies LLC) equipped with a short De Laval nozzle (Fig. 1) was employed to spray the feedstock. This gun configuration offers just enough heat for the particles to soften but not overheat. At the same time, it provides sufficient kinetic energy to the particle to stick to the surface. The torch was fueled with propane and nitrogen was used as the carrier gas.

Samples were mounted on a rotating fixture and grit-blasted using alumina powder. Next, the feedstock powder was sprayed with the process parameters mentioned in Table 2, targeting coating thicknesses of 250 μm (thick)

and 50 μm (thin). Later, the thick sprayed samples (250 μm coating) were ground to 240, 150, 100, 50 and 30 μm thickness and the thin sprayed samples (50 μm coating) were ground to 30 μm thickness (see Table 1). In this paper, the coatings with thicknesses of 30 and 50 μm are referred to as 'thin' coatings.

Characterization of Powders/Coatings

Scanning electron microscopy (SEM) was used to analyze the morphology and cross section of powder particles. For this purpose, powder particles were collected on a carbon tape and observed under SEM (HITACHI TM3000 microscope and ZEISS GeminiSEM 450). Also, for cross-sectional SEM observation, powder particles were mixed with epoxy, cold mounted, ground and polished.

Using a surface roughness tester (Surftest 301, Mitutoyo), average roughness values (R_a) of as-deposited thick and thin coatings were measured following the standard ASME B46.1. Average roughness values and respective standard deviations were calculated from three measurements on each coating.

The sprayed samples were cut and hot-mounted, then ground and polished. The grinding was performed using a 45 μm diamond disk, then polished using 9 μm and 3 μm Kemet liquid diamond solution. Then, a mirror-polished surface was obtained by employing MasterMet 2 dispense. SEM analysis was performed on the mirror-polished samples to investigate the microstructure of the sprayed coatings.

Indentation Testing

Vickers hardness of the samples was measured both on the cross section and top-surface employing Struers Duramin-40 microhardness tester. A normal load of 0.3 kgf was used for the cross-sectional hardness measurement. It should be mentioned that the cross-sectional indentations with 0.3 kgf were performed only on the coatings C30 and C240 to measure coating hardness. Also, to investigate cracking tendency of the coating, cross-sectional indentations with loads 1, 2, 3 and 4 kgf were performed on the C150 sample. To measure the hardness of coatings on the top-surface, various loads, including 0.05, 0.1, 0.2, 0.3, 0.5, 1, 2, 3 and 4 kgf, were used. For each hardness measurement, five

Fig. 1 Schematic of the nozzle used for spraying

indentations (repetitions) were performed following the standard ASTM E384 (Ref 29) and the standard deviations of the repetitions were presented using error bars. Top-surface indentation, on the other hand, was performed on all the samples (with different thicknesses) to investigate the influence of the substrate.

Ball-on-Disk Sliding Wear Testing

The same grinding and polishing procedure mentioned in Sect. Characterization of Powders/Coatings was performed on the top-surface of as-sprayed coatings to reach a mirror-polished surface for sliding wear testing. Then, sliding wear tests were carried out on the mirror-polished samples according to the ball-on-disk (BoD) testing procedure in the ASTM G99 standard (Ref 30). A tribometer rig (Tribometer TRB³, Anton-Paar, Switzerland) was employed to perform BoD tests. Coefficient of friction (CoF) was monitored throughout all the tests. The ball-on-disk tests were performed under various normal loads, including 5 N, 10 N and 20 N. For all the tests, the linear speed was set at 0.2 m/s and the total sliding distance was selected to be 5000 m. Alumina balls with a diameter of 6 mm were employed as the mating counterpart. At least two repetitions were performed for each test on radius 6 and 7 mm of wear tracks. In some cases where results from the two repetitions did not present good repeatability, a third repetition was conducted. Standard deviations of the repetitions were presented using error bars. It has been shown earlier that, for radii between 5 and 9 mm, the specific wear rate was not influenced by the testing radius (Ref 31). All the tests were conducted at room temperature.

Volume losses in the tested samples during the BoD test were measured using white light interferometry (WLI) technique by employing Profilm 3D device (Profilm 3D, Filmetrics, Germany). Since it was not feasible to capture the whole wear track, volume losses were measured at four different locations across the wear track. Based on the measured volume losses, an average cross-sectional area was obtained for the wear track and therefrom the overall volume loss of the wear track was calculated. Then, the specific wear rates for the corresponding coatings were obtained by dividing volume loss over the normal load and sliding distance. A more detailed explanation of the procedure can be found elsewhere (Ref 15, 31).

Dry Sand-Rubber Wheel Abrasion Testing

Coated rectangular plate samples were subjected to dry sand-rubber wheel abrasion tests employing an abrasion rig (abrasion tester, DUCOM, India) following the standard ASTM G-65 (Ref 32). The tests were conducted on as-sprayed samples, using SiO_2 quartz-based sand (DUCOM,
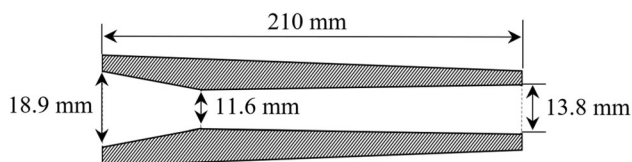
Table 1 Specification of three batches of powders with different ranges of particle size

Code	Coating thickness, μm	Samples' information
C240	240	Reached thickness by grinding and polishing identically sprayed thick coatings (250 μm)
C150	150	
C100	100	
C50	50	
C30	30	
C30-sprayed thin	30	Reached the thickness by grinding thin coating (50 μm)

India) with a particle size distribution of 100–500 μm as abrasive medium. The sand feed rate was set at 315 g/min and a normal force of 130 N was applied on the coatings to press the sample against a rubber wheel (227 mm diameter, and 13 mm width rotating at a speed of 200 rev/min). Each test was run for a total time of 30 min, with the samples being weighed at 10 min time intervals. The mass loss was measured by weighing the ultrasonically cleaned samples before and after each test using a laboratory weighing scale (PCE Deutschland GmbH) with a precision of ± 0.1 mg.

Results

Powder Characteristics

Figure 2(a) and (b) shows the morphology of the used powder. A significant portion of the powder particles exhibited an irregular shape and only the relatively larger particles were found to bear a spherical shape. A uniform distribution of fine carbide grains (sized below 2 μm) along with the binder phase (colored in dark gray) can be identified in Fig. 2(b). Figure 2(c) shows a cross-sectional SEM image of a powder particle. Cross-sectional observation of the particles confirms the uniform distribution of the two phases of binder and carbide grains. However, there were locations where the binder phase appeared to be accumulated. Cross section of irregular and spherical shape particles did not show any significant microstructure difference. It is worth mentioning that cross section of this fine powder (5–15 μm) exhibited a denser microstructure compared to the coarser powder (15–45 μm) of the same chemistry (Ref 4).

Coating Microstructure

Figure 3 shows cross-sectional SEM images of (a) thick coating, with a thickness of 250 μm, and (b) thin coating, with a thickness of 50 μm. In both cases, the coating seemed to be well-adhered to the substrate with no sign of

separation or cracks at the interface. Dark gray spots noted at the coating-substrate interface represent alumina residue left from the grit-basting process. An extremely dense microstructure was achieved in both the thin and thick coatings (Fig. 3c and d) with no distinguishable difference in their microstructure throughout the thickness. Very limited signs of pores can be detected as opposed to the coatings deposited from coarser powders which showed pores of bigger sizes and higher percentages (Ref 15). Localized regions of binder accumulation as well as the presence of fine carbide grains, both of which were noted in the starting feedstock powder (see Fig. 2c), are also clearly noted in the coating microstructure (see Fig. 3d and e). Retention of the microstructure is due to the lower flame temperature as one of the main characteristics of the HVAF process (Ref 33).

The average Ra value for the thin coating was around 1.9 ± 0.1 μm, while the value for the thick coating was slightly higher (2.2 ± 0.2 μm).

Cross-sectional and Top-Surface Hardness

Indentation tests on the cross section of the coatings (performed with a normal load of 300 gf) showed Vickers numbers of 1420 ± 29 and 1475 ± 46 for C30 and C240 coatings, respectively. The slightly lower average value of the hardness of the thin coating (C30) could be because of the influence of the softer substrate and the mounting material. For C30 coating, indent diagonals of ~ 20 μm were marked in the middle of the cross sections, which were only ~ 15 μm away from the interfaces. This was not the case for C240 samples since the coating was thick enough to locate the indents sufficiently far from the interfaces. However, these hardness values were well above the hardness of the coating fabricated from coarse powder with Vickers number of 1250 ± 45 (Ref 4). As explained in another work (Ref 15) the reason could be due to denser coating being fabricated by decrease in particle size as well as a stronger peening effect when employing finer powder.
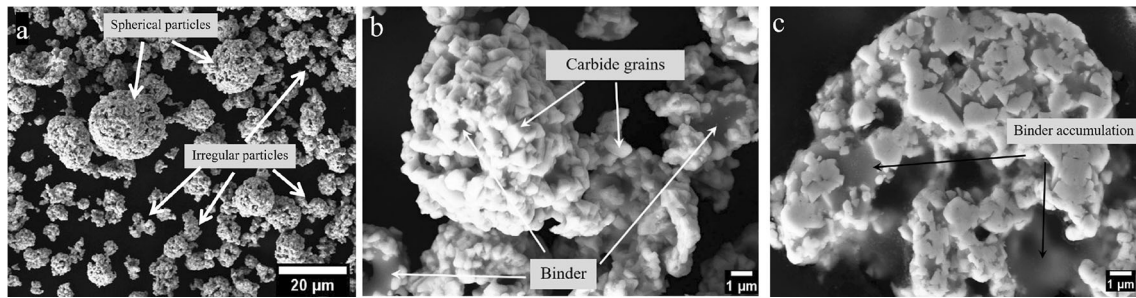
Fig. 2 SEM micrographs of (a) and (b): particle surface morphologies and (c): particle cross sections of the powder used

Fig. 3 Cross-sectional SEM micrographs of (a): thick sprayed coating, (b): thin sprayed coating and (c): typical microstructure of the thick coating at higher magnification, (d): typical microstructure of the thin coating at higher magnification, (e): typical coatings microstructure at high magnification and retention of fine carbides
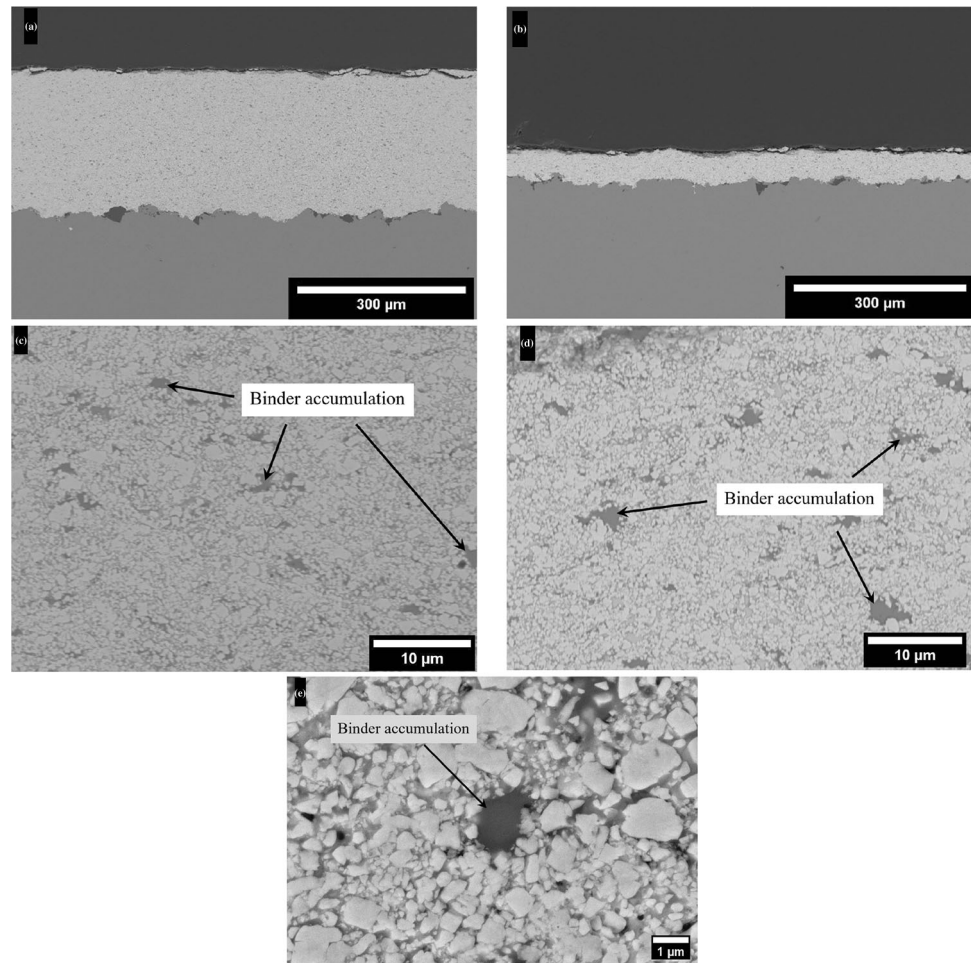
Indentation tests were also performed on the top-surface of all the samples with different thicknesses at various loads with the aim of exploring whether there is any influence of the substrate on the apparent hardness of the coatings. Figure 4 shows the scatter of apparent top-surface hardness values performed at different loads up to 4 kgf on coatings with various thicknesses ranging from 150 to 30 μm.

Apparent Vickers hardness numbers exhibited a similar trend for all C150, C100, C50 and C30 coatings, when conducted at loads up to 0.5 kgf. Average hardness values experienced a slight decreasing trend from 1500 HV0.1 to 1400 HV0.5 by increasing the normal load from 0.1 to 0.5 kgf. This slight decrease could be due to indentation size effect (Ref 34). Due to this effect, hardness values tend to increase as the indentation depth decreases. By further increasing the load from 0.5 to 1 kgf, no considerable decrease was observed for the three coatings C150 and 100 and C50. However, a clear decline from 1400 HV0.5 to 1000 HV1 was observed in C30 coating. C150 and C100

coatings experienced a further slight decrease from 1400 HV0.5 to 1330 HV4 when further increasing the load from 0.5 to 4 kgf. C50, on the other hand, showed a notable declining trend by the increase in normal load in a way that the apparent hardness value of 1270 HV2 (when performing under 2 kgf) was decreased to 1000 HV3 and 800 HV4 when increasing normal load to 3 kgf and 4 kgf, respectively. For C30 coating, this declining trend was also observed to become even more marked for higher loads with the apparent hardness value decreasing to around 490 HV2 and 350 HV3 for 2 kgf and 3 kgf, respectively (Table 2).

It is well-known that the mechanical properties (such as hardness) of a hard coating can be influenced by a softer substrate (Ref 35, 36). This effect is governed by the penetration depth of the indent and thickness of the coating in a way that by the increase in penetration depth, the influence of the substrate becomes more dominant. However, according to the empirical rule (Bückle), the influence of the substrate is avoidable if the penetration depth is less than 1/10th of the coating thickness (Ref 37). Penetration depth can be calculated based on the Vickers hardness equation explained in standard ASTM E384 (Ref 29). Table 3 presents the penetration depth of the indents performed at various loads on coatings of different thicknesses. By comparing Table 3 and Fig. 1, it can be seen that whenever the penetration depth exceeds 1/10th of the coating thickness (values in bold font), a significant drop in the apparent surface hardness value is evident, thereby reflecting the influence of the substrate. For the rest of the indents, regardless of coating thickness, the penetration depth is almost the same for a given normal load. Figures in italic font indicate values just exceeding the 1/10th threshold.

Figure 5(a), (b) and (c) shows SEM micrographs of indents on top-surface of C30 coatings corresponding to 0.5 kgf, 1 kgf and 4 kgf of normal load. In the case of 0.5

kgf normal load, no cracks or breakage of the coating was observed around the indent. By increasing the normal load from 0.5 to 1 kgf, formation of cracks, mostly within the penetration area (inside the indent, designated as I), were observed. Also, signs of limited crack propagation can be traced outside of the indent (designated as II). For the indent performed at the highest load (4 kgf), rigorous cracking occurred inside and outside the indent. In this case, the coating was greatly fractured in the form of cone-cracking, surrounding the indent. This can be due to the particular stress field in a Vickers indentation. This stress field results in great plastic deformation of the substrate under the indent, and as a result, deformation and breakage of the hard coating (Ref 38-40).

Different cracking behavior of the indents was observed when performing on the cross section. Radial in-plane cracking was indicated for loads higher than 2 kgf (Fig. 5d, e and f). No cracking was observable for the loads 1 kgf or less, while signs of crack initiation were detected at 2 kgf (Fig. 5d). The cracks were in the form of in-plane due to the presence of soft substrate and the mounting material.

Sliding Wear

Sliding wear performance of all the coatings with various thicknesses was evaluated by performing BoD testing and comparing the specific wear rate values. Also, CoF was monitored for all the tests throughout the tests and post-wear analysis was performed on the resulting wear tracks.

Figure 6(a) shows CoF evolution for the three coatings C30, C100 and C240 during BoD testing performed under 20 N as normal load. All the tests were reached a steady-state CoF after about 10,000 s of running-in period. CoF value for each test was relatively steady with limited spikes, which is usual for this type of coatings (Ref 31, 41). CoF average values for all the tests were recorded to be between 0.25 and 0.35. Under 20 N normal load, C240

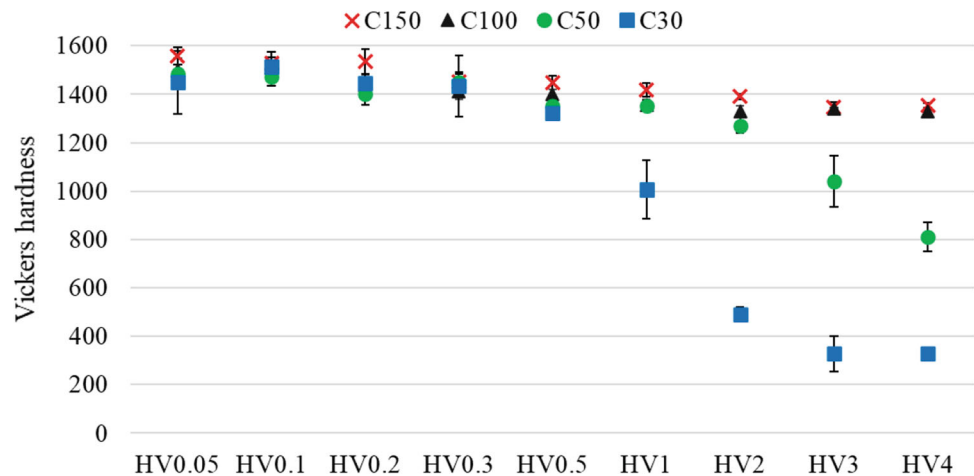Fig. 4 Apparent top-surface Vickers hardness values of all the coatings; performed at various loads

Table 2 HVAF spraying parameters employed for coating deposition

Parameter	Value
Air, psi/bar	99/6.82
Fuel, psi/bar	95/6.55
Carrier gas flow rate, l/min	40
Powder feed rate, g/min	160
Standoff distance, mm	200
The traverse speed of the spray torch, m/min	100
Carrier gas	Nitrogen

coating showed slightly lower CoF value among all, however, no clear reasoning can be suggested for this behavior since it greatly depends on the stochastic nature of the contact between the two surfaces.

Figure 6(b) presents the specific wear rates for all the coatings tested under 20 N normal load. All the coatings with various thicknesses performed outstandingly, revealing a very low specific wear rate of the order of 10^{-8} ($mm^3 \cdot N^{-1} \cdot m^{-1}$). The two coatings C240 and C150 exhibited similar performance with the average specific wear rate of around 1.5×10^{-8} ($mm^3 \cdot N^{-1} \cdot m^{-1}$). In none of the coatings, the substrate was exposed and this was

Table 3 Penetration depth of top-surface indentation (in μm) on different coatings under various loads and a comparison with 1/10 of coating thicknesses (t)

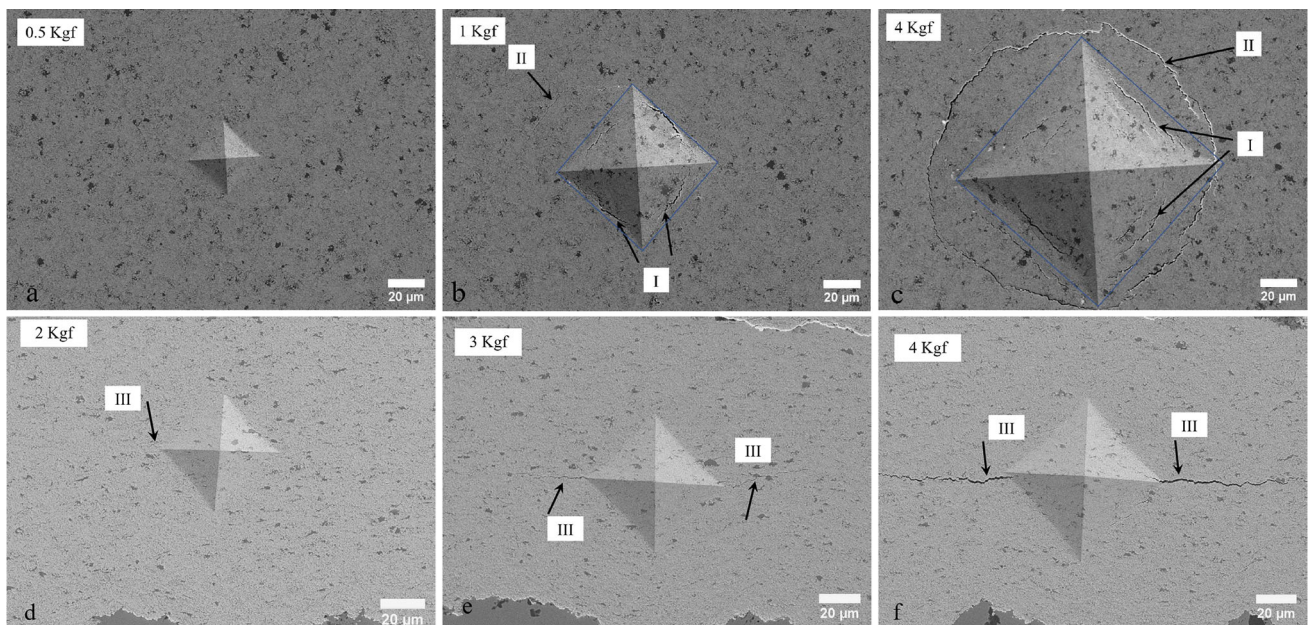|	C30 (t/10 = 3 μm)	C50 (t/10 = 5 μm)	C100 (t/10 = 10 μm)	C150 (t/10 = 15 μm)
0.05 kgf	1.1	1.1	1.1	1.1
0.1 kgf	1.6	1.6	1.6	1.6
0.2 kgf	2.3	2.3	2.3	2.2
0.3 kgf	2.8	2.8	2.8	2.8
0.5 kgf	**3.8**	3.7	3.7	3.6
1 kgf	*6.1*	**5.3**	5.3	5.2
2 kgf	*12.4*	*7.7*	7.5	7.4
3 kgf	*18.6*	*10.5*	9.2	9.2
4 kgf	*21.4*	*13.7*	**10.7**	10.6

Fig. 5 SEM micrographs of the indents performed on top-surface of C30 coatings (a, b and c) and cross section of C150 coating (d, e, and f) at various loads indicated in the pictures. Cracking tendency of the indents performed on top-surface inside and outside of the indents indicated by I and II, respectively. Cracking tendency of the indents performed on the cross section in the form of radial in-plane cracks, shown by III

expected considering the extremely low specific wear rate (see penetration depth in Fig. 10(e)). By decreasing coating thickness to 100, 50 and 30 μm, a slight increasing trend in specific wear rate was observed so that the specific wear rate of C30 coating was measured to be 4×10^{-8} (mm^3·N^{-1}·m^{-1}). To explore the possible explanation of this slight increase in specific wear rate, post-wear analysis was conducted on the as-tested C30 and C240 coatings. This is subsequently discussed in Sect. Abrasion Wear. Specific wear rates for alumina balls were measured in the case of C30 and C240. The values for the two coatings were similar with a rate of $\sim 1.6 \pm 0.1 \times 10^{-9}$ (mm^3·N^{-1}·m^{-1}). This was expected considering the same wear track width in the case of C30 and C240 coatings Fig. 10(e).

As shown in Fig. 6(b), the specific wear rate of C240 coating was higher than that of the C30 coating when testing under 20 N normal load. Figure 7(a) shows average CoF values for all the coatings after the initial running-in period (after 10,000 s), comprising standard deviation calculated from the average CoF values of test repetitions. Average CoF values fluctuate between 0.2 and 0.4 for C240 and C30 tested under 5, 10 and 20 N load. The average CoF for the C240 under 20 N was around half of the value for C30 (22 vs. 41) tested under the same load. No correlation could be found between the CoF and load for the other two coatings.

In order to investigate the possible reason for this behavior, BoD tests were performed under lower loads, including 10 N and 5 N. Figure 7(b) shows specific wear rate values for thin and thick coatings in terms of various normal loads. Under 5 N of normal load, C30 performed even slightly superior to the thick coating. Also, for the case of 10 N normal load, the wear performance of the two thick and thin coatings was comparable. Hence, it can be concluded that wear performance of thick and thin coatings is similar under BoD testing when the normal load is 10 N or less. In other words, when surface pressure is less than a

certain value, the tribological behavior of the coatings was similar and not significantly influenced by their thickness. To confirm this, another suitable tribological test was selected, with less surface pressure, to evaluate the performance of the thin and thick coatings. In abrasion testing, under standard ASTM G65, contact pressure is expected to be lower because of the distribution of normal load over a larger area of the surface.

Abrasion Wear

Figure 8 shows weight loss of C240 and C30 coatings along with results from another thick WC-CoCr coating fabricated from coarse powder (15–45 μm) under sand-rubber wheel testing during three time intervals of 10 min. Reasonably constant slopes for both the tests indicate that the tests reached steady-state situation from the very beginning of the first 10 min, and also reflect the repeatability of the tests. In the case of thick coating fabricated from coarse powder, Thick-Coarse, it can be seen that, unlike C30 and C240, the steady-state situation was not achieved and mass loss shows a decreasing trend, with the mass loss during the first 10 min being higher (Ref 4). The reason could be the rougher surface finish in the case of coatings fabricated from the coarse powder (see Sect. Coating Microstructure) and the consequent preferential removal of the significant surface asperities during the early stages of testing. A similar slope and, as a result, an almost identical total mass loss at the end of the tests suggested comparable abrasion wear performance of the thick and thin coatings.

Influence of Peening Effect

It was shown that both thick (C240) and thin (C30) coatings performed comparable under reasonably milder surface pressure. However, all the coatings discussed thus far
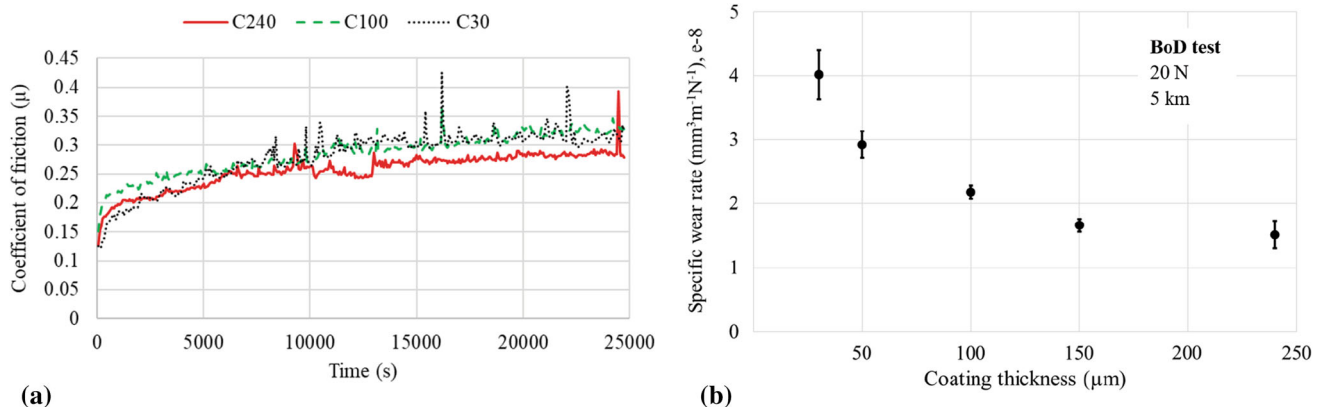

Fig. 6 Wear results for coatings tested under 20 N normal load, (a): CoF evolution throughout the tests for C30, C100 and C240 coatings, (b): specific wear rate values for all the coatings
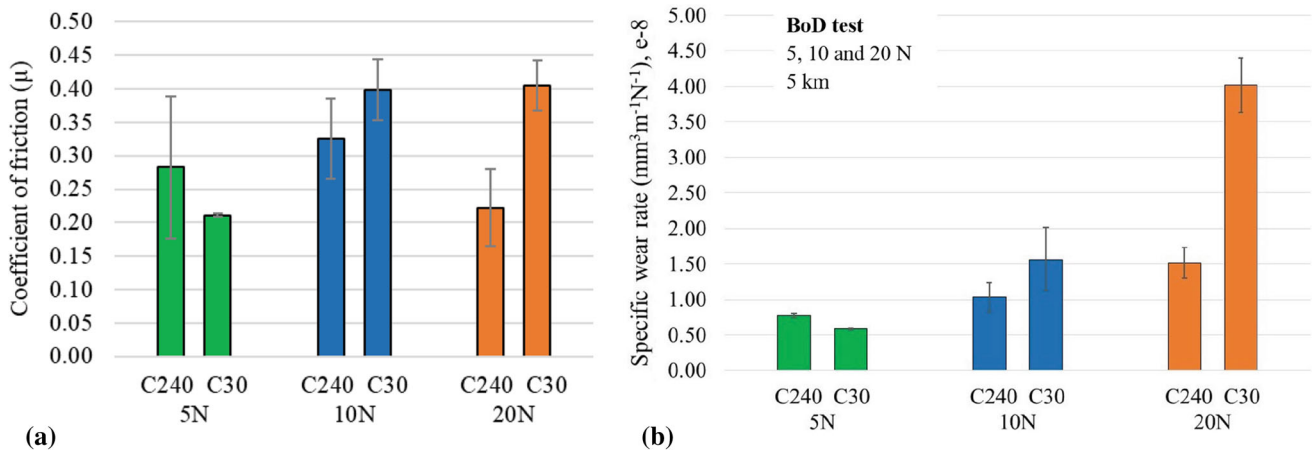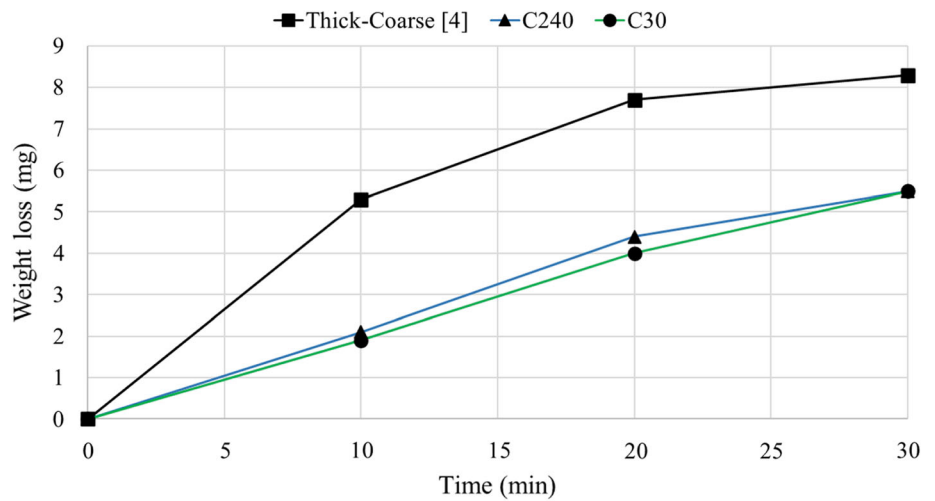
Fig. 7 Wear results for C240 and C30 coatings tested under 20 N, 10 N and 5 N normal load, (a): average value of CoF value during steady and (b): specific wear rate values

Fig. 8 Abrasion wear performance of the thick (C240) and thin (C30) coatings along with the thick coating fabricated from coarse powder (Ref 4)

were first sprayed thick to an identical thickness (about 250 microns) and then ground to different thicknesses. The motivation for this was to prevent any deviation in coating microstructure or properties originating from a potential difference in the spraying process. However, in HVAF-sprayed WC-based coatings, considerable potential compressive stresses are expected due to the peening effect. Besides, the induced compressive residual stresses increase with coating thickness and this is attributable to the progressively higher number of particle impacts. Moreover, the underlying coating during each spraying scan is subjected to a peening effect (Ref 42–44). Therefore, a thin coating ground from an initial thick coating (C30) can potentially represent different properties than a thin coating which was originally sprayed thin (C30-sprayed thin specimen), if the role of peening is significant. Hence, the tribological behavior of these coatings should be separately evaluated.

Figure 9 shows the specific wear rate of the two C30 and C30_sprayed thin coatings. Comparable performance of the two coatings can be concluded. This result can rule out the possible influence of the peening effect on wear performance of the WC-CoCr coatings fabricated from fine powder feedstock. This result aligns with a negligible difference in the microstructure of the two coatings, as discussed in Sect. Coating Microstructure. This observation is in contrast with the results in the study by Bolelli et al. (Ref 28), in which the peening effect and consequent densification were suggested to be responsible for a better wear performance in thicker HVOF-sprayed (2 torch scans vs. 5 torch scans) WC-CoCr coarse (from powder size of 15–45 μm) coatings. However, this contradiction can be originated from the difference in spraying techniques employed (i.e., HVAF vs. HVOF). For the case of HVOF coatings, it was observed that the coatings become denser and harder by increasing the number of torch scans (Ref

28). While in the HVAF case (this study), no clear difference was observed in the coating microstructure when changing thickness. In other words, the coating is already pretty dense for peening not to have such a significant role in the densification of sub-layers.

Discussion

It was seen that for 20 N normal load, a clear decline occurred in wear performance of the thin coatings. There could be two possible reasons for this decline: i) influence of peening or compressive residual stresses and ii) influence of the substrate. The peening effect can be considered negligible from various points of view. Firstly, in Fig. 6, it can be seen that the two coatings C240 and C150 (which is C240 polished to 150 μm) performed the same, although most top layers of the coating ground down to 150 μm from about 250 μm in case of C150 have undergone more strokes and as a result more peening effect than the C240 coating. Besides, considering that peening results in a more densified microstructure, the performance should have experienced an improvement. While according to Fig. 6, the wear performance declines by moving toward layers that have undergone more stroke scans (less thickness). Moreover, it is clearly shown in Fig. 9 that C30 (sprayed 250 μm and ground to 30 μm), with a higher peening effect, performed similar to C30_sprayed thin (sprayed 50 μm and ground to 30 μm), with a lower peening effect, which again confirms the negligible influence of peening here. The negligible difference in hardness value (under lower loads than 0.5 kgf) of the thin and thick coatings as well as coating microstructure throughout the thickness are the other reaffirmations of this.

Substrate, on the other hand, was found to have a great influence on apparent surface hardness as well as wear

performance under certain testing conditions. According to the Hertzian theory of contact mechanics for sphere on a flat surface (Ref 45), the contact radius a_r, the average Hertzian contact stress σ_{avg}, the maximum Hertzian contact stress σ_{max} and the maximum shear stress τ_{max} can be calculated using Eqs. 1, 3, 4 and 5.

$$a_r = \left(\frac{3F_n R}{4E_r}\right)^{1/3} \tag{Eq 1}$$

$$\frac{1}{E_r} = \frac{1 - v_b^2}{E_b} + \frac{1 - v_c^2}{E_c} \tag{Eq 2}$$

$$\sigma_{avg} = \frac{F_n}{\pi a_r^2} \tag{Eq 3}$$

$$\sigma_{max} = \frac{3}{2}\sigma_{avg} \tag{Eq 4}$$

$$\tau_{max} = \frac{F_n}{2\pi a_r^2} \tag{Eq 5}$$

where F_n is the applied normal load, R is radius of the ball as the counterpart, E_r is reduced Young's modulus, E_b and E_c are the Young's modulus of the ball and the coating, respectively, and v_b and v_c are the Poisson's ratios of the ball and the coating, respectively. Maximum shear stress occurs at a depth of z below the surface according to Eq. 6 (Ref 46).

$$z = 0.638a_r \tag{Eq 6}$$

Calculated values for the average Hertzian contact stress, the maximum Hertzian contact stress, the maximum shear stress and the corresponding depth at the beginning of the test are presented in Table 4. The calculation was done based on the following mechanical properties for the coating and the alumina ball as the counterpart: E_c = 257 GPa, v_c = 0.28 (Ref 47), E_b = 370 GPa and v_b = 0.22 (Ref 48).

According to Table 4, location of the maximum shear stress for loads 5 N, 10 N and 20 N occurs at 19 μm, 25 μm and 31 μm from the surface, respectively. It is clear that by increasing normal load not only the Hertzian stress is increased but the location of maximum shear stress is also moved toward the substrate. Meaning that in the case
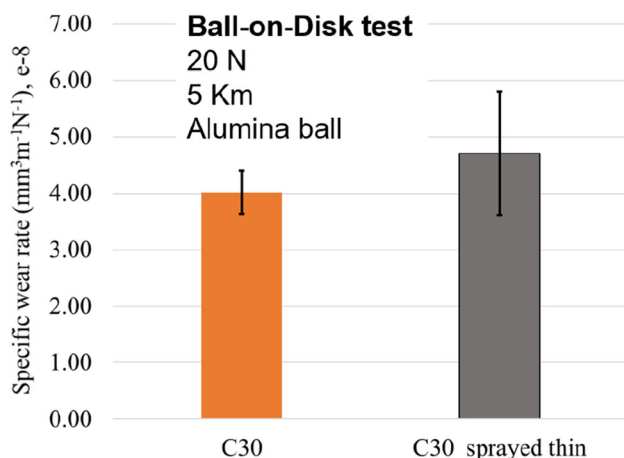
Fig. 9 Wear results for C30 and C30_sprayed thin coatings

Table 4 Average Hertzian contact stress σ_{avg}, maximum Hertzian contact pressure σ_{max}, maximum shear stress τ_{max} and the corresponding depth z

F_n, N	σ_{avg}, GPa	σ_{max}, GPa	τ_{max}, GPa	z, μm
5	0.94	1.41	0.44	19
10	1.18	1.78	0.56	25
20	1.49	2.24	0.70	31

Fig. 10 Post-wear analysis of tested C30 (thin) and C240 (thick) coatings, (a), (c): optical images of wear tracks, (b), (d): SEM micrographs of wear tracks; (e): Wear track profiles
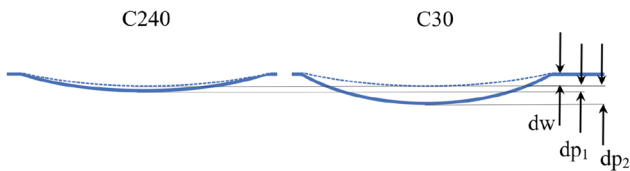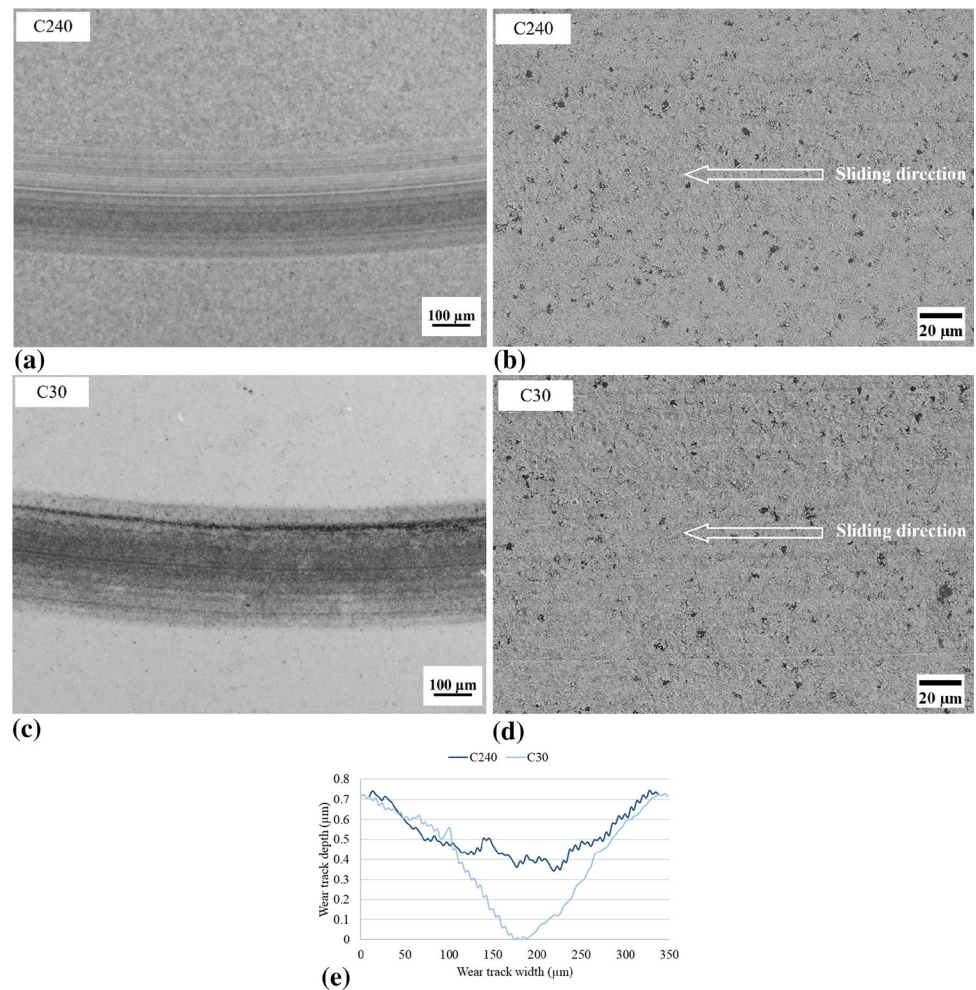

Fig. 11 Schematic diagram of wear tracks of C240 and C30 coatings under 20 N normal load
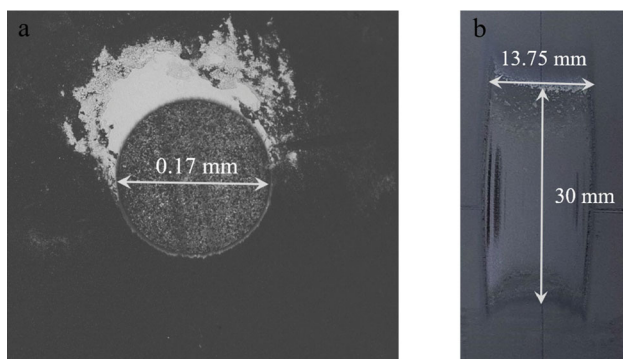

Fig. 12 Contact surface in the wear tests (a): ball in sliding wear and (b): coating tested under abrasion wear

of thinner coatings under higher loads, most of the load is to be carried by the substrate (soft) and as a result, plastic deformation of the substrate and the coating. This can explain the jump in specific wear rate in case of C30 when testing under 20 N normal load (see Fig. 7b), where the maximum shear stress is close or within the substrate. However, no big difference was observed in wear mechanisms of thin and thick coatings, as shown in Fig. 10. Instead, it seems that in the case of C30 coating, the coating material was more plastically deformed, or in other word, the ball was more sank into the surface. This results in a deeper wear track for coatings C30 while the width of the wear tracks is similar (see Fig. 10e).

In other words, for thinner coatings, when the normal load (surface pressure) exceeds a certain value, the apparent surface hardness declines because of substrate influence. This suggests the surface being apparently softer and easier to penetrate. Figure 11 shows a schematic view of wear tracks under 20 N normal load. In both cases, some material is removed (dw) which can be considered roughly the same for the two thick and thin coatings. On the other

hand, in both cases, material can be plastically deformed (dp_1 and dp_2) which itself is correlated to the apparent hardness of the surface. In the case of C30, apparent hardness is lower and higher penetration depth is expected compared to the coating C240 ($dp_2 > dp_1$). Surface hardness investigation in Sect. Cross-sectional and Top-Surface Hardness confirms lower apparent hardness of the thinner coatings when the surface load exceeds a certain limit.

To further affirm the influence of high surface pressure and as a result, involvement of substrate, a rough calculation was made for the surface pressure in the cases of sliding wear and abrasion wear and they were compared to a real application.

Figure 12 shows contact surfaces in BoD and abrasion after the tests are finished. Normal pressure on the coatings can be calculated by having area of the contact surface and considering the normal load of 20 N for BoD and 130 N for abrasion (at the end of the tests). Normal pressure of at least 220 MPa was applied in the case of BoD testing, while this value for abrasion was only about 0.3 MPa. Also, according to Table 4, average Hertzian contact stresses of 0.94 GPa, 1.18 GPa and 1.49 GPa are applied to the coating/substrate (at the beginning of the sliding wear testing) under 5 N, 10 N and 20 N load, respectively. However, it is very unusual to find an application where Hertzian stress surpasses 1 GPa (Ref 47). For instance, one of the applications of WC-based coatings could be automotive breaking disks (Ref 49). Normal pressure in an automotive braking disk was calculated to give an idea of surface pressure in a typical real application. The surface area of a typical braking pad is around 9,000 mm^2 and the normal load can be in a range of 5 to 15 kN (Ref 50). Thus, the normal pressure was calculated to be in a range of 0.5 to 1.6 MPa. Therefore, it can be seen that normal pressure in a BoD testing with 20 N normal load can be far more severe compared to some of the real applications. Hence, thinner WC-based coatings can be considered a promising route to save operation costs as well as the usage of conflict elements such as W and Co in the applications where the surface pressure is not very extreme.

Summary and Conclusions

Tribological performance of HVAF-sprayed WC-CoCr coatings was evaluated under sliding and abrasion wear conditions. Also, microstructural and mechanical characteristics of the coatings were studied in order to better explain the wear behavior of the deposited coatings. It can be concluded that;

- Microstructure and hardness of the thick and thin coatings seemed to be comparable without any noticeable difference.
- Sliding wear performance of the coatings with thicknesses lower than 150 μm, under 20 N normal load, showed to be slightly inferior to that of conventional thick coatings. By further investigation, performing hardness measurements at various loads, calculating values and locations of the Hertzian contact stresses as well as BoD tests at lower loads, it was concluded that the severe high pressure (> 1 Gpa Hertzian stress) and as a result influence of substrate is the reason of slight decline in wear performance of thinner coatings under BoD test with 20 N normal load.
- Thin and thick coatings exhibited similar performance when testing under sliding wear with a normal load of 10 N or lower. Also, the apparent top-surface hardness of all the coatings was similar for the load of 0.5 kgf or lower.
- Sprayed thick and sprayed thin coatings showed similar performance under sliding wear conditions, indicating a negligible peening effect influence.

References

1. A. Vardelle, C. Moreau, J. Akedo, H. Ashrafizadeh, C.C. Berndt, J.O. Berghaus, M. Boulos, J. Brogan, A.C. Bourtsalas, A.

Dolatabadi, M. Dorfman, T.J. Eden, P. Fauchais, G. Fisher, F. Gaertner, M. Gindrat, R. Henne, M. Hyland, E. Irissou, E.H. Jordan, K.A. Khor, A. Killinger, Y.C. Lau, C.J. Li, L. Li, J. Longtin, N. Markocsan, P.J. Masset, J. Matejicek, G. Mauer, A. McDonald, J. Mostaghimi, S. Sampath, G. Schiller, K. Shinoda, M.F. Smith, A.A. Syed, N.J. Themelis, F.L. Toma, J.P. Trelles, R. Vassen and P. Vuoristo, The Thermal Spray Roadmap, *J. Therm. Spray Technol.*, 2016, **25**(2016), p 1376-1440. https://doi.org/10.1007/s11666-016-0473-x

2. K. Torkashvand, S. Joshi, M. Gupta, Advances in Thermally Sprayed WC-Based Wear-Resistant Coatings: Co-free Binders, Processing Routes and Tribological Behavior, J. Therm. Spray Technol. (2022) 1-36.

3. O. Aranke, W. Algenaid, S. Awe and S. Joshi, Coatings for Automotive Gray Cast Iron Brake Discs: A Review, *Coatings*, 2019, **9**, p 1-31. https://doi.org/10.3390/coatings9090552

4. K. Torkashvand, S. Joshi, V. Testa, F. Ghisoni, S. Morelli, G. Bolelli, L. Lusvarghi, F. Marra and M. Gupta, Tribological Behavior of HVAF-Sprayed WC-Based Coatings with Alternative Binders, *Surf. Coat. Technol.*, 2022, **436**, 128296.

5. L.-M. Berger, Coatings by Thermal Spray, *Compr. Hard Mater.*, 2014, **1**, p 471-506.

6. L.-M. Berger, S. Saaro, T. Naumann, M. Kašparova and F. Zahálka, Influence of Feedstock Powder Characteristics and Spray Processes on Microstructure and Properties of WC–(W, Cr) 2C–Ni Hardmetal Coatings, *Surf. Coatings Technol.*, 2010, **205**, p 1080-1087.

7. H. Myalska, L. Lusvarghi, G. Bolelli, P. Sassatelli and G. Moskal, Tribological Behavior of WC-Co HVAF-Sprayed Composite Coatings Modified by Nano-Sized TiC Addition, *Surf. Coatings Technol.*, 2019, **371**, p 401-416. https://doi.org/10.1016/j.surfcoat.2018.09.017

8. X.T. Luo, G.M. Smith, Y. Wang, E. Gildersleeve, S. Sampath and C.J. Li, Cracking Induced Tribological Behavior Changes for the HVOF WC-12Co Cermet Coatings, *Ceram. Int.*, 2019, **45**, p 4718-4728. https://doi.org/10.1016/j.ceramint.2018.11.164

9. R.R. White, Tuneable high velocity thermal spray gun, (1995).

10. A new research and innovation infrastructure of Forschungszentrum Jülich, (2020). https://www.fz-juelich.de/iek/iek-1/DE/Forschung/JuelichThermalSprayCenter/JTSC_FZJ.html.

11. A. Hamilton, A. Sharma and U. Pandel, Solid Particle Erosion Resistance of HVAF-Sprayed Wc-10Co-4Cr Coating on Ca6Nm Steel, *Surf Rev Lett*, 2017 https://doi.org/10.1142/S0218625X18500117

12. B. Huang, C. Zhang, G. Zhang and H. Liao, Wear and Corrosion Resistant Performance of Thermal-Sprayed Fe-Based Amorphous Coatings: A Review, *Surf. Coatings Technol.*, 2019, **377**, 124896. https://doi.org/10.1016/j.surfcoat.2019.124896

13. A. Ghabchi, Wear resistant carbide-based thermal sprayed coatings: process, properties, mechanical degradation and wear, PhD Thesis. (2011).

14. H. Kreye, High velocity oxy-fuel flame spraying-state of art, new developments and alternatives, in: Tagungsunterlagen Conf. Proceedings, Erding, 2003, (2003).

15. K. Torkashvand, M. Gupta, S. Björklund, F. Marra, L. Baiamonte and S. Joshi, Influence of Nozzle Configuration and Particle Size on Characteristics and Sliding Wear Behaviour of HVAF-Sprayed WC-CoCr Coatings, *Surf. Coatings Technol.*, 2021, **423**, p 127585.

16. Q. Wang, S. Zhang, Y. Cheng, J. Xiang, X. Zhao and G. Yang, Wear and Corrosion Performance of WC-10Co4Cr Coatings Deposited by Different HVOF and HVAF Spraying Processes, *Surf. Coatings Technol.*, 2013, **218**, p 127-136. https://doi.org/10.1016/j.surfcoat.2012.12.041

17. V. Testa, S. Morelli, G. Bolelli, B. Benedetti, P. Puddu, P. Sassatelli and L. Lusvarghi, Alternative Metallic Matrices for WC-Based HVOF Coatings, *Surf. Coatings Technol.*, 2020, **402**, 126308.

18. M.L. Grilli, D. Valerini, R.R. Piticescu, T. Bellezze, M. Yilmaz, A. Rinaldi, S. Cuesta-López and A. Rizzo, Possible Alternatives to Critical Elements in Coatings for Extreme Applications, *IOP Conf. Ser. Mater. Sci. Eng.*, 2018 https://doi.org/10.1088/1757-899X/329/1/012005

19. A.H. Tkaczyk, A. Bartl, A. Amato, V. Lapkovskis and M. Petranikova, Sustainability Evaluation of Essential Critical Raw Materials: Cobalt, Niobium, Tungsten and Rare Earth Elements, *J. Phys. D. Appl. Phys.*, 2018, **51**(20), p 203001. https://doi.org/10.1088/1361-6463/aaba99

20. WHO, IARC Monographs on the evaluation of carcinogenic risks to humans. Cobalt in Hard Metals and Cobalt Sulfate, Gallium Arsenide, Indium Phosphide and Vanadium Pentoxide, World Heal. Organ. Int. Agency Reserach Cancer, Lyon Fr. 86 (2006) 3-5.

21. National Institutes of Health (NIH), Report on Carcinogens Trichloroethylene, (2016). https://ntp.niehs.nih.gov/whatwestudy/assessments/cancer/roc/index.html?utm_source=direct&utm_medium=prod&utm_campaign=ntpgolinks&utm_term=roc.

22. C. Lyphout, G. Bolelli, E. Smazalova, K. Sato, J. Yamada, Š Houdková, L. Lusvarghi and T. Manfredini, Influence of Hardmetal Feedstock Powder on the Sliding Wear and Impact Resistance of High Velocity Air-Fuel (HVAF)Sprayed Coatings, *Wear*, 2019, **430–431**, p 340-354. https://doi.org/10.1016/j.wear.2019.05.016

23. G. Bolelli, L.-M.M. Berger, T. Börner, H. Koivuluoto, L. Lusvarghi, C. Lyphout, N. Markocsan, V. Matikainen, P. Nylén, P. Sassatelli, R. Trache and P. Vuoristo, Tribology of HVOF- and HVAF-Sprayed WC – 10Co4Cr Hardmetal Coatings: A Comparative Assessment, *Surf. Coatings Technol.*, 2015, **265**, p 125-144. https://doi.org/10.1016/j.surfcoat.2015.01.048

24. Z. Piao, B. Xu, H. Wang and C. Pu, Effects of Thickness and Elastic Modulus on Stress Condition of Fatigue-Resistant Coating Under Rolling Contact, *J. Cent. South Univ. Technol.*, 2010, **17**, p 899-905.

25. K. Holmberg, H. Ronkainen and A. Matthews, Tribology of Thin Coatings, *Ceram. Int.*, 2000, **26**, p 787-795.

26. R. Ahmed and M. Hadfield, Failure Modes of Plasma Sprayed WC–15% Co Coated Rolling Elements, *Wear*, 1999, **230**, p 39-55.

27. A. Nakajima, T. Mawatari, M. Yoshida, K. Tani and A. Nakahira, Effects of Coating Thickness and Slip Ratio on Durability of Thermally Sprayed WC Cermet Coating in Rolling/Sliding Contact, *Wear*, 2000, **241**, p 166-173.

28. G. Bolelli, L. Lusvarghi and M. Barletta, HVOF-Sprayed WC–CoCr Coatings on Al alloy: Effect of the Coating Thickness on the Tribological Properties, *Wear*, 2009, **267**, p 944-953.

29. A. ASTM, Standard test method for microindentation hardness of materials, ASTM Int. West Conshohocken. (2011).

30. ASTM International, Standard Test Method for Wear Testing with a Pin-on-Disk Apparatus G99–17, *Annu. B. ASTM Stand.*, 2017, **05**, p 1-6. https://doi.org/10.1520/G0099-17.Copyright

31. K. Torkashvand, V.K. Selpol, M. Gupta and S. Joshi, Influence of Test Conditions on Sliding Wear Performance of High Velocity Air Fuel-Sprayed WC–CoCr Coatings, *Materials (Basel).*, 2021, **14**, p 3074.

32. ASTM G65–16, Standard Test Method for Measuring Abrasion Using the Dry Sand/Rubber Wheel Apparatus, ASTM B. Stand. Vol. 03.02. (2021). https://doi.org/10.1520/G0065-16R21.

33. G. Bolelli, L.M. Berger, T. Börner, H. Koivuluoto, L. Lusvarghi, C. Lyphout, N. Markocsan, V. Matikainen, P. Nylén, P. Sassatelli, R. Trache and P. Vuoristo, Tribology of HVOF- and HVAF-sprayed WC-10Co4Cr Hardmetal Coatings: A

Comparative Assessment, *Surf. Coatings Technol.*, 2015, **265**, p 125-144. https://doi.org/10.1016/j.surfcoat.2015.01.048

34. A. Iost and R. Bigot, Indentation Size Effect: Reality or Artefact?, *J. Mater. Sci.*, 1996, **31**, p 3573-3577.

35. F. Cleymand, O. Ferry, R. Kouitat, A. Billard and J. von Stebut, Influence of Indentation Depth on the Determination of the Apparent Young's Modulus of Bi-Layer Material: Experiments and Numerical Simulation, *Surf. Coatings Technol.*, 2005, **200**, p 890-893. https://doi.org/10.1016/j.surfcoat.2005.02.086

36. M.G.J. Veprek-Heijman and S. Veprek, The Deformation of the Substrate During Indentation into Superhard Coatings: Bückle's Rule Revised, *Surf. Coatings Technol.*, 2015, **284**, p 206-214. https://doi.org/10.1016/j.surfcoat.2015.10.064

37. J.H. Westbrook, The science of hardness testing and its research applications, (1973).

38. K. Holmberg, A. Laukkanen, H. Ronkainen, K. Wallin, S. Varjus and J. Koskinen, Tribological Contact Analysis of a Rigid Ball Sliding on a Hard Coated Surface: Part II: Material Deformations, Influence of Coating Thickness and Young's Modulus, *Surf. Coatings Technol.*, 2006, **200**, p 3810-3823.

39. E. Broitman, Indentation Hardness Measurements at Macro-, Micro-, and Nanoscale: A Critical Overview, *Tribol. Lett.*, 2017, **65**, p 1-18. https://doi.org/10.1007/s11249-016-0805-5

40. Y. Kadin, M. Mazaheri, V. Zolotarevskiy, C. Vieillard and M. Hadfield, Finite Elements Based Approaches for the Modelling of Radial Crack Formation Upon Vickers Indentation in Silicon Nitride Ceramics, *J. Eur. Ceram. Soc.*, 2019, **39**, p 4011-4022. https://doi.org/10.1016/j.jeurceramsoc.2019.05.058

41. G. Bolelli, L.-M. Berger, T. Börner, H. Koivuluoto, V. Matikainen, L. Lusvarghi, C. Lyphout, N. Markocsan, P. Nylén and P. Sassatelli, Sliding and Abrasive Wear Behaviour of HVOF-and HVAF-Sprayed Cr_3C_2–NiCr Hardmetal Coatings, *Wear*, 2016, **358**, p 32-50.

42. R. Ahmed, O. Ali, C.C. Berndt and A. Fardan, Sliding Wear of Conventional and Suspension Sprayed Nanocomposite WC-Co Coatings: An Invited Review, *J. Therm. Spray Technol.*, 2021, **30**(4), p 800-861.

43. G. Bolelli, I. Hulka, H. Koivuluoto, L. Lusvarghi, A. Milanti, K. Niemi and P. Vuoristo, Properties of WC – FeCrAl Coatings Manufactured by Different High Velocity Thermal Spray Processes, *Surf. Coat. Technol.*, 2014, **247**, p 74-89. https://doi.org/10.1016/j.surfcoat.2014.03.021

44. T. Varis, T. Suhonen, M. Jokipii and P. Vuoristo, Surface & Coatings Technology Influence of Powder Properties on Residual Stresses Formed in High-Pressure Liquid Fuel HVOF Sprayed WC-CoCr Coatings, *Surf. Coat. Technol.*, 2020, **388**, 125604. https://doi.org/10.1016/j.surfcoat.2020.125604

45. K.L. Johnson and K.L. Johnson, *Contact mechanics*, Cambridge University Press, Cambridge, 1987.

46. G.W. Stachowiak and A.W. Batchelor, *Engineering tribology*, Butterworth-heinemann, Oxford, 2013.

47. G. Bolelli, V. Cannillo, L. Lusvarghi and T. Manfredini, Wear Behaviour of Thermally Sprayed Ceramic Oxide Coatings, *Wear*, 2006, **261**, p 1298-1315.

48. Matweb, Mechanical Properties, (2022). https://www.matweb.com/search/DataSheet.aspx?MatGUID=c8c56ad547ae4cfabad15977bfb537f1&ckck=1.

49. O. Aranke, W. Algenaid, S. Awe, S. Joshi, Thermal Spray Coatings for Automotive Gray Cast Iron Brake Discs: A Review, Materials (Basel). (2019) 1-31.

50. Brembo, Brake pad, (2022). https://www.bremboparts.com/asiapacific/en/catalogue/pad/P_44_023.